

A Spatial-Domain Coordinated Control Method for Connected and Automated Vehicles at Unsignalized Intersections Considering Motion Uncertainty

Tong Zhao, Nikolce Murgovski, and Wei ShangGuan, *Member, IEEE*

Abstract—Cooperative driving of connected and automated vehicles (CAVs) emerges as a promising solution to enhance traffic safety, efficiency, and sustainability. Meanwhile, mixed traffic, where CAVs coexist with conventional human-driven vehicles (HDVs), represents an upcoming and necessary stage in the development of intelligent transportation systems. Considering the motion uncertainty of HDVs, this paper proposes a coordinated control method for trajectory planning of CAVs at an unsignalized intersection in mixed traffic. By sampling in distance and using an exact change of variables, the coordinated control problem is formulated as a nonlinear program in the spatial domain, thereby allowing for unified linear collision avoidance constraints to handle crossing, following, merging, and diverging vehicle conflicts. The motion uncertainty of HDVs is decoupled and modeled as path uncertainty and speed uncertainty, whereby the robustness of collision avoidance is ensured in both spatial and temporal dimensions. The prediction deviation for HDVs is compensated by receding horizon optimization, and a real-time iteration (RTI) scheme is developed to improve computational efficiency. Simulation case studies are conducted to validate the efficacy, robustness, and potential for real-time application of the proposed method. The results show that the proposed control scheme provides collision-free and smooth trajectories with state and control constraints satisfied. Compared with the converged baseline, the RTI scheme reduces the computation time by a factor of 111 on average, and the solution deviation is less than 2.26%, demonstrating a good trade-off between computational effort and optimality.

Index Terms—Connected and automated vehicles (CAVs), coordinated control, trajectory planning, nonlinear optimization, model predictive control (MPC), unsignalized intersections.

I. INTRODUCTION

A. Motivation

CONNECTED and automated vehicles (CAVs) are considered one of the disruptive technologies that are expected to change the transportation landscape [1], [2]. With the aid

This work was supported in part by the Joint Fund of the Ministry of Education for Equipment Pre-Research under Grant 8091B022238; in part by the Beijing Outstanding Young Scientists Program under Grant JWZQ20240101010; and in part by the China Scholarship Council under Grant 202307090098. (*Corresponding author: Wei ShangGuan.*)

Tong Zhao is with the School of Automation and Intelligence, Beijing Jiaotong University, Beijing 100044, China (e-mail: tong_zhao@bjtu.edu.cn).

Nikolce Murgovski is with the Department of Electrical Engineering, Chalmers University of Technology, 412 96 Gothenburg, Sweden (e-mail: nikolce.murgovski@chalmers.se).

Wei ShangGuan is with the School of Automation and Intelligence, the State Key Laboratory of Advanced Rail Autonomous Operation, and the Research Center for Autonomous Intelligence and Unmanned Systems, Beijing Jiaotong University, Beijing 100044, China (e-mail: wshg@bjtu.edu.cn).

of vehicle-to-everything (V2X) communication, CAVs are able to achieve cooperative driving, which holds great potential for improving traffic safety, efficiency, and sustainability [3], [4].

Unsignalized intersections, being common and prone to crashes and congestion [5], [6], have been widely regarded as typical application scenarios for cooperative driving [7]. Various methods and techniques have been proposed for cooperative decision-making and control of CAVs at unsignalized intersections [8], [9], [10], [11]. However, most of them only work for fully cooperative systems with 100% CAV penetration. Over a long period of time, CAVs and conventional human-driven vehicles (HDVs) will coexist and thus constitute mixed traffic, which is an inevitable stage in the evolution of intelligent transportation systems towards full autonomy. Therefore, it is significant to consider the motion uncertainty of HDVs and investigate coordinated control methods for CAVs applicable to unsignalized intersections in mixed traffic.

B. Literature Review

From the perspective of research ideas, existing approaches to cooperative driving at unsignalized intersections can be classified into two categories: 1) one-stage approaches, which directly solve for the trajectories of CAVs; 2) two-stage approaches, which decouple the cooperative driving problem into two parts: crossing scheduling and trajectory planning, and first schedule the crossing order of all vehicles, and then plan the trajectories of CAVs based on this. The one-stage approach tends to embed complex safety constraints, resulting in a highly nonlinear and nonconvex optimization problem that is difficult to solve [12], [13], [14]. In contrast, the two-stage approach reduces the problem complexity through decoupling and provides the flexibility that each stage can be handled by different methods. In the following, we focus on the research progress of the two-stage approach.

In terms of crossing scheduling, some strategies determine the crossing order based on heuristic rules, e.g., resource reservation [15], service auction [16]. Such schemes can be implemented quickly online, but their solutions are not guaranteed to be optimal or good enough. Another class of strategies solves for the optimal crossing order by constructing an optimization problem, typically a mixed-integer linear program [17], [18]. However, the computational complexity increases dramatically with the problem size, making these strategies intractable for real-time applications. To balance the computational effort and optimality, heuristic optimization scheduling algorithms based

on Monte Carlo tree search have been developed [19], [20]. In addition, deep reinforcement learning techniques have been utilized to improve scheduling adaptability [21]. Despite the fruitful results, most of the existing studies have not considered the motion uncertainty of HDVs, which is one of the key factors affecting the feasibility of the crossing order under mixed traffic. In this regard, game-theoretic scheduling methods have been proposed for exploration [22], [23]. However, it is still extremely challenging to properly model heterogeneous vehicle interactions with uncertainty, followed by efficiently searching for the optimal crossing order.

In terms of trajectory planning, the basic idea is to construct and solve optimal control problems (OCPs) with objectives such as time efficiency, comfort, and energy saving, to generate physically constrained and collision-free acceleration or velocity profiles for CAVs, while ensuring that the scheduled crossing order is followed. One approach is to formulate continuous OCPs and derive analytic solutions using Hamiltonian analysis to compute CAV trajectories in a sequential distributed fashion [24], [25]. However, in order to fulfill the control and state constraints, multiple cases have to be discussed sequentially for each CAV trajectory computation, which can be time-consuming; moreover, analytic solutions are not guaranteed to be derived when the constraints or cost functions are complex. A more common approach is to formulate discrete OCPs and solve them numerically using existing optimization methods; both centralized [26], [27], [28] and distributed [29], [30], [31]. For example, Hult et al. introduced time variables to express the collision avoidance constraints as state couplings between different vehicles, planned CAV trajectories by solving a nonlinear program (NLP) [26], and proposed a semi-distributed solution to improve computational efficiency [32]. In [29], attraction sets were derived using reachability analysis tools to estimate potential collision times, and CAV trajectories were obtained by sequentially solving a set of quadratic programs (QPs). Zhang et al. [33] first centrally formulated non-overlapping spatio-temporal corridors as collision avoidance domains, and then computed trajectories for each CAV in a parallel distributed manner. In [34], collision-free trajectories were trained offline based on iterative learning for different crossing modes. Distinguishing from the above studies oriented to fully CAV conditions, in [35], CAVs in entry lanes were controlled to coordinate mixed platoons, with the assumption that HDVs are guided by advanced driver assistance systems. In [36], CAVs were coordinated under mixed traffic using model predictive control (MPC), and the infeasibility problem due to HDV uncertainty was addressed by relaxing a portion of the collision avoidance constraints.

Overall, the research on coordinated trajectory planning at unsignalized intersections is impressive, but the following shortcomings remain.

- 1) To comprehensively address vehicle crossing, following, merging, and diverging conflicts at unsignalized intersections, time-dependent collision avoidance constraints are often complex and nonconvex, making the OCP difficult to solve [37]. A common response is to simplify such constraints by pre-estimating the relevant time variables [38], [39]; however, additional steps are required and both

feasibility and optimality suffer.

- 2) The related work for mixed traffic is quite scarce, especially in terms of robust collision avoidance that takes into account the motion uncertainty of HDVs.
- 3) In response to the problem of different speed limits on straights and curves, most existing studies deal with the straight ahead and turning processes separately, an approach that lacks optimality.
- 4) Anchoring the temporal control horizon is tricky when the travel times of CAVs are optimization variables rather than specified values [40], [41]. The vast majority of existing studies empirically set temporal control horizons for specific cases, which is clearly not suitable for practical applications.

C. Contribution of the Paper

In this paper, we propose a coordinated centralized MPC for trajectory planning of CAVs at an unsignalized intersection in mixed traffic. By sampling in distance and using an exact change of variables, the coordinated control problem is defined in the spatial domain rather than in the temporal domain as in most existing studies, thus establishing convex collision avoidance constraints without approximation and eliminating the horizon anchoring problem. A motion prediction model with uncertainty for HDVs is developed, and prediction deviations are compensated via MPC. This work is an extension of the previous study in [27], which was limited to open-loop control for vehicle crossing scenarios under fully CAV conditions. The main contributions of this paper are summarized as follows.

- 1) The coordinated control problem is formulated as an NLP in the spatial domain, which expresses the collision avoidance constraints for vehicle crossing, following, merging, and diverging in a unified linear form, and is able to handle spatially varying speed limits linearly.
- 2) The motion uncertainty of HDVs is decoupled and modeled as path uncertainty and speed uncertainty, whereby the robustness of collision avoidance is ensured in both spatial and temporal dimensions.
- 3) A real-time iteration (RTI) scheme is developed for efficient implementation of MPC, which achieves a good trade-off between computational effort and optimality.

D. Organization of the Paper

The remainder of this paper is organized as follows. Section II formulates the coordinated control problem at an unsignalized intersection under mixed traffic in the temporal domain. In Section III, the problem formulation is transformed from the temporal domain to the spatial domain, the motion uncertainty of HDVs is modeled, robust collision avoidance constraints are established, and the coordinated control problem is reformulated as an NLP. In Section IV, the NLP is deployed in the MPC framework, cost functions are presented, and an RTI scheme is developed for efficient computation. Section V demonstrates the efficacy of the proposed methods through simulation case studies. Finally, concluding remarks and future plans are given in Section VI.

II. PROBLEM FORMULATION

This paper focuses on the coordinated control of CAVs at an unsignalized intersection in mixed traffic, i.e., traffic with both CAVs and HDVs. In this section, we introduce the intersection scenario, model the vehicle kinematics, and formulate the coordinated control problem.

A. Unsignalized Intersections

Mathematically, any unsignalized intersection can be represented by the tuple

$$(p, x_l(p), y_l(p), \kappa_l(p), \psi_l(p), v_l^s(p), \mathcal{L}), \quad (1)$$

where p is a sampling variable denoting the distance traveled along the path, $x_l(p)$, $y_l(p)$ are the global coordinates of the predefined path $l \in \mathcal{L}$ at sample p , and $\kappa_l(p)$, $\psi_l(p)$, and $v_l^s(p)$ are the path curvature, tangent angle, and speed limit, respectively.

As a typical example, consider the four-way unsignalized intersection shown in Fig. 1, where vehicles are allowed to go straight, turn left, or turn right in the central area, depicted in gray. Each link consists of one entry lane and one exit lane, with the direction of travel shown by the arrows. Each entry lane derives three paths leading to each exit lane that is not part of the same link as that entry lane, resulting in a total of 12 predefined paths. Finally, the red circle marks the control boundary, within which any vehicle is considered part of the intersection.

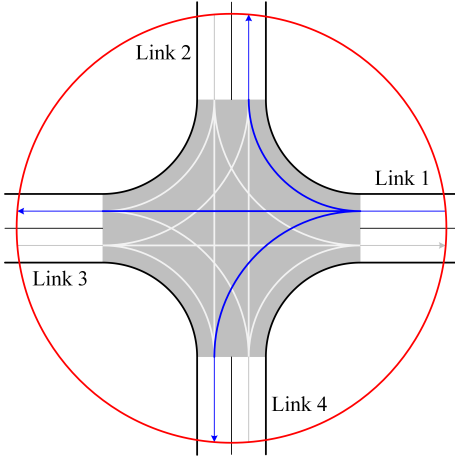


Fig. 1. An unsignalized intersection with four links, each with one entry lane and one exit lane. There are a total of 12 predefined paths, and the three paths starting from the first link are depicted in blue. The gray area is the central area. The red circle indicates the control boundary.

Now, consider $N \geq 1$ vehicles, consisting of M CAVs, with $1 \leq M \leq N$, and $N - M$ HDVs, traveling through the intersection, and assume that

- the crossing order has been given by a high-level scheduling module;
- the states (location, speed, etc.) of all vehicles can be captured at any time;
- the turning intentions of all vehicles are known and do not change;
- all CAVs are under centralized control;

- communication delays are negligible;
- lane changing is prohibited.

In practical terms, HDVs are sensed by CAVs and roadside units (RSUs), traffic information is shared through V2X communication, and centralized control is served by a certain CAV or RSU.

The set of all vehicle indexes is denoted as $\mathcal{N} = \{1, \dots, M, \dots, N\}$, and its subset $\mathcal{M} = \{1, \dots, M\}$ is defined as the set of CAV indexes, and thus the set of HDV indexes is $\mathcal{N} \setminus \mathcal{M}$. Note that the intersection illustrated in Fig. 1 is only an example used herein, and the methods herein can be applied to unsignalized intersections with different geometries.

B. Vehicle Paths

It is assumed that each vehicle $i \in \mathcal{N}$ is following a reference path

$$\mathbf{p}_{ir}(p) = [p \ x_{ir}(p) \ y_{ir}(p) \ \kappa_{ir}(p) \ \psi_{ir}(p) \ v_{ir}^s(p)], \quad (2)$$

which is one of the predefined paths, i.e., $\mathbf{p}_{ir}(p) = [p \ x_l(p) \ y_l(p) \ \kappa_l(p) \ \psi_l(p) \ v_l^s(p)]$ for some $l \in \mathcal{L}$. Thereby, the path of vehicle i can be expressed as

$$\begin{aligned} \mathbf{p}_i(p) &= [p \ x_i(p) \ y_i(p) \ \kappa_i(p) \ \psi_i(p) \ v_i^s(p)] \\ &= \mathbf{p}_{ir}(\tilde{p}) + \mathbf{w}_i(\tilde{p}), \quad \mathbf{w}_i(\tilde{p}) \in \mathcal{W}_i(\tilde{p}), \quad \tilde{p} \in [\tilde{p}_{i0}, \tilde{p}_{if}], \end{aligned} \quad (3)$$

where \tilde{p} is the projection of sample p onto the reference path, $\mathbf{w}_i(\tilde{p})$ is the path-following deviation of vehicle i and its range $\mathcal{W}_i(\tilde{p})$ is a complete bounded subset of \mathbb{R}^6 , and \tilde{p}_{i0} and \tilde{p}_{if} are the projections of the initial position p_{i0} and the final position p_{if} of vehicle i onto the reference path, respectively. Furthermore, CAVs are assumed to follow their respective reference paths perfectly, i.e., $\mathcal{W}_i(\tilde{p}) \equiv \{\mathbf{0}\}$ for all $i \in \mathcal{M}$. In contrast, the path-following deviations of HDVs are non-negligible and uncertain.

C. Longitudinal Kinematics

For each vehicle $i \in \mathcal{N}$, let $\mathbf{x}_i(t) = [p_i(t) \ \dot{p}_i(t)]^\top$ denote its state vector, where t is the time, and $p_i(t)$ and $\dot{p}_i(t)$ are the longitudinal position and longitudinal velocity along its path, respectively. Then, vehicle i is represented by a linear system

$$\dot{\mathbf{x}}_i(t) = \mathbf{A}\mathbf{x}_i(t) + \mathbf{B}u_i(t), \quad (4)$$

with

$$\mathbf{A} = \begin{bmatrix} 0 & 1 \\ 0 & 0 \end{bmatrix}, \quad \mathbf{B} = \begin{bmatrix} 0 \\ 1 \end{bmatrix}, \quad (5)$$

where the longitudinal acceleration along its path is chosen as the control signal, i.e., $u_i(t) = \ddot{p}_i(t)$.

D. State and Control Constraints

Each CAV $i \in \mathcal{M}$ is subject to state and control constraints

$$\mathbf{x}_i(t) \in [\mathbf{x}_i^{\min}, \mathbf{x}_i^{\max}(p_i(t))], \quad (6)$$

$$u_i(t) \in [u_i^{\min}, u_i^{\max}], \quad (7)$$

where the inequalities are imposed for all $t \in [0, t_{if}]$ and

$$\mathbf{x}_i^{\min} = [p_{i0} \ 0]^\top, \quad \mathbf{x}_i^{\max}(p_i(t)) = [p_{if} \ v_i^{\max}(p_i(t))]^\top. \quad (8)$$

The final time t_{if} , when CAV i reaches its final position p_{if} , is free.

Unlike going straight, when a vehicle turns left or right, it moves on a path segment with significant curvature. In this case, the vehicle is subjected to non-negligible lateral forces, which should be limited to an acceptable level for driving safety and comfort. Since the lateral forces mainly provide centripetal acceleration, the maximum longitudinal velocity of CAV i is given as

$$v_i^{\max}(p_i(t)) = \min \left\{ v_i^s(p_i(t)), \sqrt{a_{in}^{\max}/\kappa_i(p_i(t))} \right\}, \quad (9)$$

where a_{in}^{\max} is the maximum acceptable centripetal acceleration of CAV i .

E. Problem Statement

Coordinated control aims to enable CAVs to safely, efficiently, and smoothly pass through unsignalized intersections in mixed traffic. For each vehicle $i \in \mathcal{N}$, let $\mathbf{x}_{i0} = [p_{i0} \ v_{i0}]^\top$ and $\mathbf{x}_{if} = [p_{if} \ \text{free}]^\top$ denote its initial and final states, respectively. Then, in the temporal domain, the coordinated control problem for CAVs is formulated as

$$\min_{\mathbf{u}_c, \mathbf{t}_{cf}} \sum_{i=1}^M J_i(\mathbf{x}_i(t), u_i(t), \dot{u}_i(t), t_{if}) \quad (10a)$$

subject to

$$\dot{\mathbf{x}}_i(t) = A\mathbf{x}_i(t) + Bu_i(t), \quad \forall i \in \mathcal{N}, \quad (10b)$$

$$\mathbf{x}_i(t) \in [\mathbf{x}_i^{\min}, \mathbf{x}_i^{\max}(p_i(t))], \quad \forall i \in \mathcal{M}, \quad (10c)$$

$$u_i(t) \in [u_i^{\min}, u_i^{\max}], \quad \forall i \in \mathcal{M}, \quad (10d)$$

$$h(\mathbf{x}, \mathbf{u}_c, \mathbf{u}_H, \mathbf{w}) \leq 0, \quad \forall \mathbf{u}_H \in \mathcal{U}_H, \quad \forall \mathbf{w} \in \mathcal{W}, \quad (10e)$$

$$\mathbf{x}_i(0) = \mathbf{x}_{i0}, \quad \mathbf{x}_i(t_{if}) = \mathbf{x}_{if}, \quad \forall i \in \mathcal{N}, \quad (10f)$$

where the constraints (10b)-(10d) are imposed for all $t \in [0, t_{if}]$. The optimization variables are the control signals and final times of all CAVs, i.e., $\mathbf{u}_c = [u_1(t) \ \dots \ u_M(t)]$ and $\mathbf{t}_{cf} = [t_{1f} \ \dots \ t_{Mf}]$, while those of all HDVs are uncertain variables. The robust constraint (10e) describes the collision avoidance conditions both between CAVs and between CAVs and HDVs, where $\mathbf{x} = [\mathbf{x}_1^\top(t) \ \dots \ \mathbf{x}_N^\top(t)]$ and $\mathbf{w} = [\mathbf{w}_1(\tilde{p}_1(t)) \ \dots \ \mathbf{w}_N(\tilde{p}_N(t))]$ represent the state vectors and path-following deviations of all vehicles, respectively, with \mathbf{w} ranging over some bounded set \mathcal{W} , and \mathbf{u}_H represents the control signals of all HDVs, which belongs to some bounded set \mathcal{U}_H . The cost function $J_i(\cdot)$ for each CAV $i \in \mathcal{M}$ may include penalties for deviation from the reference speed, for the control signal, for changes in the control signal, for the final time, for the final state, etc. The detailed implementation of the cost function is deferred to Section IV-B.

It can be seen that the collision avoidance constraint (10e) is the core of the optimization problem (10). However, the explicit expression of the constraint (10e) in the temporal domain is often nonconvex and, due to the uncertainty involved in the motion of HDVs, complex in form. Furthermore, since the upper speed bound (9) is decision-variable dependent, the state constraints (10c) tend to be nonlinear and nonconvex. In addition, anchoring the temporal control horizon is tricky

because the final times \mathbf{t}_{cf} are optimization variables. These make problem (10) difficult to solve. Therefore, in the following section, we reformulate problem (10) as a standard NLP in the spatial domain.

III. MODELING OF CONFLICT RESOLUTION CONSIDERING MOTION UNCERTAINTY

In this section, we transform the problem formulation from the temporal domain to the spatial domain using a non-approximate change of variables. Based on this, the motion uncertainty of HDVs is modeled, and robust collision avoidance constraints are further established. Finally, the coordinated control problem (10) is reformulated as an NLP.

A. Temporal-Spatial Domain Transformation

From a spatial perspective, the vehicle path is sampled in distance via the sampling variable p , while the travel time for the vehicle to reach any subsequent sample is unknown. In view of this, for each vehicle $i \in \mathcal{N}$, its travel time, $t_i(p)$, is chosen as a state and satisfies $t_i'(p) = 1/v_i(p)$. Here, the shorthand notation $(\cdot)'$ denotes the derivative with respect to distance, i.e., $(\cdot)' = d(\cdot)/dp$, and $v_i(p)$ is the speed of vehicle i at sample p . Further, the variable representing the inverse vehicle speed, $z_i(p) = 1/v_i(p)$, is introduced as another state, which is referred to as lethargy, as in [27]. Now, with $\tilde{\mathbf{x}}_i(p) = [t_i(p) \ z_i(p)]^\top$ as the state vector, vehicle i can be represented in the spatial domain by the linear system

$$\tilde{\mathbf{x}}_i'(p) = A\tilde{\mathbf{x}}_i(p) + B\tilde{u}_i(p), \quad (11)$$

where the spatial derivative of lethargy is chosen as the control signal, i.e., $\tilde{u}_i(p) = z_i'(p)$, and the matrices A and B remain as in (5).

For each CAV $i \in \mathcal{M}$, the state constraints in the spatial domain are expressed as

$$\tilde{\mathbf{x}}_i(p) \in [\tilde{\mathbf{x}}_i^{\min}(p), \tilde{\mathbf{x}}_i^{\max}], \quad (12)$$

where the inequalities are imposed for all $p \in [p_{i0}, p_{if}]$ and

$$\tilde{\mathbf{x}}_i^{\min}(p) = [0 \ 1/v_i^{\max}(p)]^\top, \quad \tilde{\mathbf{x}}_i^{\max} = [\infty \ \infty]^\top. \quad (13)$$

Here, with the same principle as in (9), the maximum speed of CAV i is given as

$$v_i^{\max}(p) = \min \left\{ v_i^s(p), \sqrt{a_{in}^{\max}/\kappa_i(p)} \right\}. \quad (14)$$

To obtain the limits of the spatial control signal, let $a_i(p) \in [a_i^{\min}, a_i^{\max}]$ denote the acceleration of CAV i at sample p , with $a_i^{\min} \leq 0$ and $a_i^{\max} \geq 0$. Observe that

$$\tilde{u}_i(p) = z_i'(p) = \left(\frac{1}{v_i(p)} \right)' = -\frac{v_i'(p)}{v_i^2(p)} = -v_i'(p)z_i^2(p), \quad (15)$$

$$v_i'(p) = \frac{d}{d(t_i(p))} v_i(p) \cdot \frac{d}{dp} t_i(p) = a_i(p)z_i(p),$$

which can be combined to derive $\tilde{u}_i(p) = -a_i(p)z_i^3(p)$. Thus, the exact translation of the control constraints into the spatial domain is given as

$$\tilde{u}_i(p) \in z_i^3(p) [-a_i^{\max}, -a_i^{\min}], \quad (16)$$

where the inequalities are imposed for all $p \in [p_{i0}, p_{if}]$.

Also, the initial and final states of each vehicle $i \in \mathcal{N}$ are translated into the spatial domain as $\tilde{\mathbf{x}}_{i0} = [0 \quad 1/v_{i0}]^\top$ and $\tilde{\mathbf{x}}_{if} = [\text{free} \quad \text{free}]^\top$, respectively.

B. Motion Uncertainty Modeling

The motion uncertainty of HDVs is reflected in both path and speed, which affect the location and timing of potential collisions. Taking the scenario depicted in Fig. 2 as an example, the left-turning HDV 4 may not strictly follow the reference path, but rather its possible paths are contained within an uncertainty set, as shown in the shaded area. Thereby, the collision location between CAV 1 and HDV 4 is uncertain, which is intuitively manifested by the non-fixation of the path conflict point. In contrast, since CAVs are assumed to follow their respective reference paths perfectly, the collision locations between them are predetermined.

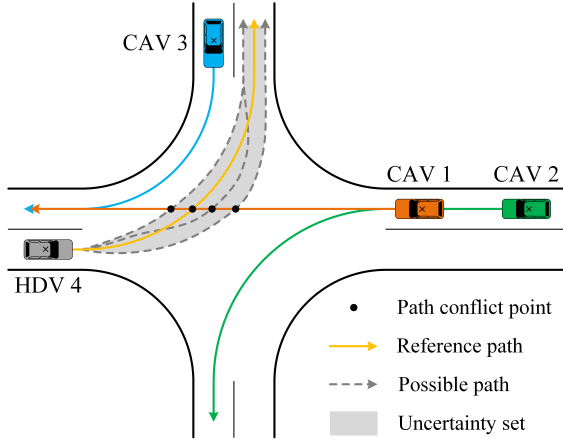


Fig. 2. Vehicles traveling through an unsignalized intersection. Each vehicle has a given reference path, depicted by a solid line with an end arrow. CAVs are assumed to follow their respective reference paths perfectly, while HDVs may not. The gray dashed lines indicate some of the possible paths of HDV 4, which are contained within an uncertainty set, depicted by the shaded area. The path conflict point between CAV 1 and HDV 4 is not fixed.

As described in Section II-B, the path of each vehicle $i \in \mathcal{N}$ can be expressed as $\mathbf{p}_i(p) = \mathbf{p}_{ir}(\tilde{p}) + \mathbf{w}_i(\tilde{p})$, where $\mathbf{w}_i(\tilde{p}) \in \mathcal{U}_i(\tilde{p})$ and $\tilde{p} \in [\tilde{p}_{i0}, \tilde{p}_{if}]$. According to the projective geometry, the tangent vector at projection \tilde{p} is denoted as $\boldsymbol{\tau}_i(\tilde{p}) = [\cos \psi_{ir}(\tilde{p}) \quad \sin \psi_{ir}(\tilde{p})]$, and the vector from projection \tilde{p} to sample p is denoted as $\mathbf{n}_i(\tilde{p}, p) = [x_i(p) - x_{ir}(\tilde{p}) \quad y_i(p) - y_{ir}(\tilde{p})]$, with $\boldsymbol{\tau}_i(\tilde{p}) \cdot \mathbf{n}_i(\tilde{p}, p) = 0$, as shown in Fig. 3. From this, given the initial coordinates $x_i(p_{i0})$, $y_i(p_{i0})$ of vehicle i , the lower bound \tilde{p}_{i0} of the projection variable \tilde{p} can be calculated, while the upper bound \tilde{p}_{if} is obviously the length of the reference path. Further, let the offset, $\xi_i(\tilde{p})$, of vehicle i with respect to the reference path characterize its path uncertainty, defined as

$$\begin{aligned} \xi_i(\tilde{p}) &= \|\mathbf{n}_i(\tilde{p}, p)\| \cdot \text{sgn}_v(\boldsymbol{\tau}_i(\tilde{p}), \mathbf{n}_i(\tilde{p}, p)), \\ \xi_i(\tilde{p}) &\in \mathcal{U}_i(\tilde{p}), \quad \tilde{p} \in [\tilde{p}_{i0}, \tilde{p}_{if}], \end{aligned} \quad (17)$$

where $\text{sgn}_v(\cdot)$ is a sign function with value domain $\{-1, 1\}$, $\xi_i(\tilde{p}) < 0$ means that the offset is clockwise, $\xi_i(\tilde{p}) > 0$ means that the offset is counterclockwise, and the path uncertainty

set $\mathcal{U}_i(\tilde{p})$ is a complete bounded subset of \mathbb{R} . For each HDV $i \in \mathcal{N} \setminus \mathcal{M}$, $\mathcal{U}_i(\tilde{p})$ is modeled based on its initial offset and road geometry, see Appendix A; while for each CAV $i \in \mathcal{M}$, $\mathcal{U}_i(\tilde{p}) \equiv \{0\}$.

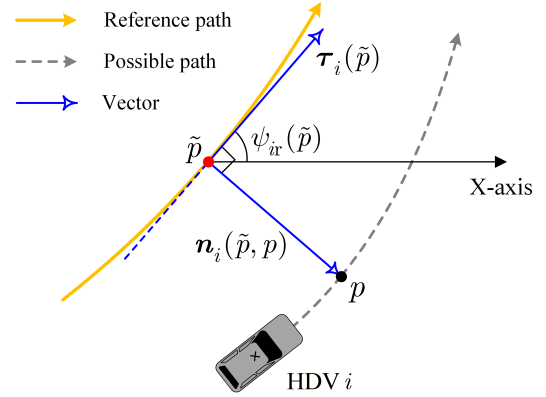


Fig. 3. Schematic of the path projection. The black dot indicates a sample and the red dot indicates the projection of that sample onto the reference path.

For ease of presentation, let the initial position of each HDV $i \in \mathcal{N} \setminus \mathcal{M}$ be $p_{i0} = \tilde{p}_{i0}$. Based on the kinematics (11), the speed of HDV i is estimated as

$$\hat{v}_i(p) = \min\{\max\{\alpha, \bar{v}_i(p)\}, \beta_i \hat{v}_i^{\max}(p)\}, \quad (18)$$

where α is a suitably small positive constant used as the lower limit of the speed estimate to avoid numerical problems due to excessively large values of lethargy, $\beta_i = \max\{1, v_{i0}/\hat{v}_i^{\max}(p_{i0})\}$ is the relaxation factor for the upper limit of the speed estimate, and

$$\hat{v}_i^{\max}(p) = \min\left\{v_{ir}^s(\tilde{p}), \sqrt{\hat{a}_{in}^{\max}/\kappa_{ir}(\tilde{p})}\right\}, \quad (19)$$

$$\bar{p} = \min\{p, \tilde{p}_{if}\},$$

$$\bar{v}_i(p) = \sqrt{2 \int_{p_{i0}}^p \gamma_i(s) ds + v_{i0}^2}, \quad \gamma_i(p) \in \Gamma_i(p). \quad (20)$$

Here, s is the integral variable corresponding to the sampling variable p , and $\gamma_i(p)$ is the perturbed acceleration of HDV i , whose range $\Gamma_i(p)$ is a complete bounded subset of \mathbb{R} . The upper limit of the speed estimate, $\hat{v}_i^{\max}(p)$, is derived by approximating the actual path speed limit and curvature to those of the reference path, as in (19), and is corrected in (18) by the relaxation factor β_i .

Further, the travel time for HDV i to reach the normal at projection \tilde{p} is estimated as

$$\begin{aligned} \hat{t}_i(\tilde{p}) &= \int_{p_{i0}}^{\tilde{p} + \omega_i(\tilde{p})} \frac{1}{\hat{v}_i(p)} dp, \quad \omega_i(\tilde{p}) \in \Omega_i(\tilde{p}), \\ \hat{t}_i(\tilde{p}) &\in [\hat{t}_i^{\min}(\tilde{p}), \hat{t}_i^{\max}(\tilde{p})], \quad \tilde{p} \in [\tilde{p}_{i0}, \tilde{p}_{if}], \end{aligned} \quad (21)$$

where $\omega_i(\tilde{p})$ is the travel distance deviation of HDV i with respect to the reference path, i.e., $p = \tilde{p} + \omega_i(\tilde{p})$, and its range $\Omega_i(\tilde{p})$ is a complete bounded subset of \mathbb{R} . From (18)-(21), it can be seen that the uncertainty in the travel time of HDV i is jointly characterized by the travel distance deviation $\omega_i(\tilde{p})$ and the perturbed acceleration $\gamma_i(p)$. Moreover,

the minimum travel time estimate, $\hat{t}_i^{\min}(\tilde{p})$, is obtained by making $\omega_i(\tilde{p}) = \min \Omega_i(\tilde{p})$ and $\gamma_i(p) = \max \Gamma_i(p)$, and the maximum travel time estimate, $\hat{t}_i^{\max}(\tilde{p})$, is obtained by making $\omega_i(\tilde{p}) = \max \Omega_i(\tilde{p})$ and $\gamma_i(p) = \min \Gamma_i(p)$.

C. Robust Collision Avoidance Constraints

Vehicle collisions may occur where paths intersect, overlap, or approach, which are referred to as critical zones. The collision avoidance constraints can be imposed by constraining the time when CAVs enter and exit the critical zone so that it is occupied by at most one vehicle.

Let $O \in \mathcal{N}^N$ represent a given vehicle crossing order, which is a specific permutation of all the elements in \mathcal{N} , and let O_i denote the order of vehicle i in O . Considering the physical dimensions and safety margins of the vehicle, let $\mathcal{B}_i(\tilde{p}, \xi_i(\tilde{p}))$ denote the bounding box of vehicle i with projection \tilde{p} and offset $\xi_i(\tilde{p})$, which is set to be a rectangle, and the heading angle of vehicle i is approximated to be $\psi_{ir}(\tilde{p})$. Then, for vehicle i and vehicle j with $O_i < O_j$, the possible collision locations are given as

$$\begin{aligned} \mathcal{P}_{ij} = \{ & (\tilde{p}_1, \tilde{p}_2) \in [\tilde{p}_{i0}, \tilde{p}_{if}] \times [\tilde{p}_{j0}, \tilde{p}_{jf}] \mid \mathcal{B}_i(\tilde{p}_1, \xi_i(\tilde{p}_1)) \\ & \cap \mathcal{B}_j(\tilde{p}_2, \xi_j(\tilde{p}_2)) \neq \emptyset, \xi_i(\tilde{p}_1) \in \mathcal{U}_i(\tilde{p}_1), \\ & \xi_j(\tilde{p}_2) \in \mathcal{U}_j(\tilde{p}_2), O_i < O_j, (23) \}, \end{aligned} \quad (22)$$

$$\nexists O_i < O_m < O_j, \mathbf{p}_{mr}(p) = \mathbf{p}_{ir}(p) \vee \mathbf{p}_{mr}(p) = \mathbf{p}_{jr}(p), \quad (23)$$

where $\mathcal{B}_i(\cdot) \cap \mathcal{B}_j(\cdot) \neq \emptyset$ means that the bounding box of vehicle i overlaps with that of vehicle j , which is regarded as a collision. The overlap determination is achieved using the separating axis theorem. The condition (23) is used to ensure the compactness of potential collision identification. For example, in vehicle following, it is not necessary to consider collision avoidance with vehicles other than the immediate leader.

To identify the critical zones for vehicle i and vehicle j , suppose that the collision location \tilde{p}_2 of vehicle j is the entrance of some critical zone. Then the exit is given by

$$f(\tilde{p}_2) = \max\{\tilde{p}_1 \mid (\tilde{p}_1, \tilde{p}_2) \in \mathcal{P}_{ij}\}. \quad (24)$$

Suppose that the collision location \tilde{p}_1 of vehicle i is the exit of some critical zone. Then the entrance is given by

$$g(\tilde{p}_1) = \min\{\tilde{p}_2 \mid (\tilde{p}_1, \tilde{p}_2) \in \mathcal{P}_{ij}\}. \quad (25)$$

Thus, the critical zones can be represented by their exit and entrance locations

$$\mathcal{C}_{ij} = \{(\tilde{p}_{\text{out}}, \tilde{p}_{\text{in}}) \in \mathcal{P}_{ij} \mid \tilde{p}_{\text{out}} = f(\tilde{p}_{\text{in}}), \tilde{p}_{\text{in}} = g(\tilde{p}_{\text{out}})\}. \quad (26)$$

Now, the collision avoidance constraints can be expressed as linear constraints

$$\begin{aligned} t_{ij}(\tilde{p}_{\text{out}}, \tilde{p}_{\text{in}}) + \lambda_{ij}(\tilde{p}_{\text{in}}) &\leq -t_j^{\text{des}}, \lambda_{ij}(\tilde{p}_{\text{in}}) \in [-t_j^{\text{des}}, 0], \\ \forall (\tilde{p}_{\text{out}}, \tilde{p}_{\text{in}}) \in \mathcal{C}_{ij}, \forall i, j \in \mathcal{N}, \{i, j\} &\not\subseteq \mathcal{N} \setminus \mathcal{M}, \end{aligned} \quad (27)$$

where $\lambda_{ij}(\cdot)$ is the slack variable introduced to avoid infeasibility problems caused by motion prediction deviations for HDVs, t_j^{des} is the positive, desired time gap of vehicle j , and

$$t_{ij}(\tilde{p}_{\text{out}}, \tilde{p}_{\text{in}}) = \begin{cases} \hat{t}_i^{\max}(\tilde{p}_{\text{out}}) - t_j(\tilde{p}_{\text{in}}), & \text{if } i \in \mathcal{N} \setminus \mathcal{M}, j \in \mathcal{M}, \\ t_i(\tilde{p}_{\text{out}}) - \hat{t}_j^{\min}(\tilde{p}_{\text{in}}), & \text{if } i \in \mathcal{M}, j \in \mathcal{N} \setminus \mathcal{M}, \\ t_i(\tilde{p}_{\text{out}}) - t_j(\tilde{p}_{\text{in}}), & \text{if } i, j \in \mathcal{M}. \end{cases} \quad (28)$$

These constraints state that vehicle i must exit the critical zone before vehicle j enters it, for which the slack variable $\lambda_{ij}(\cdot)$ receives a substantial penalty in the objective function. Moreover, the constraints are robust because the edge cases of both collision location and collision timing are covered. As an example, the traffic conflict between CAV 1 and HDV 4 in Fig. 2 is depicted in detail as shown in Fig. 4. It can be seen that the path uncertainty of HDV 4 is reflected in its bounding box, which becomes wider as the path uncertainty increases. If CAV 1 is specified to pass after HDV 4, i.e., $O_4 < O_1$, then $(\tilde{p}_{4,3}, \tilde{p}_{1,1})$ and $(\tilde{p}_{4,4}, \tilde{p}_{1,2})$ are the only two critical zones plotted in Fig. 4, which cover all the other plotted collision locations such as $(\tilde{p}_{4,1}, \tilde{p}_{1,4})$ and $(\tilde{p}_{4,2}, \tilde{p}_{1,3})$. Similarly, if CAV 1 is specified to pass before HDV 4, i.e., $O_1 < O_4$, then $(\tilde{p}_{1,4}, \tilde{p}_{4,1})$ and $(\tilde{p}_{1,5}, \tilde{p}_{4,2})$ are the only two critical zones plotted in Fig. 4. This indicates that the identified critical zones are full-coverage, ensuring the robustness of collision avoidance in the spatial dimension, and are also non-redundant. For the timing of HDVs entering and exiting the critical zone, the worst-case scenario is always considered to ensure the robustness of collision avoidance in the temporal dimension. As in (28), if an HDV is specified to go first, its maximum travel time estimate is adopted; otherwise, its minimum travel time estimate is adopted.

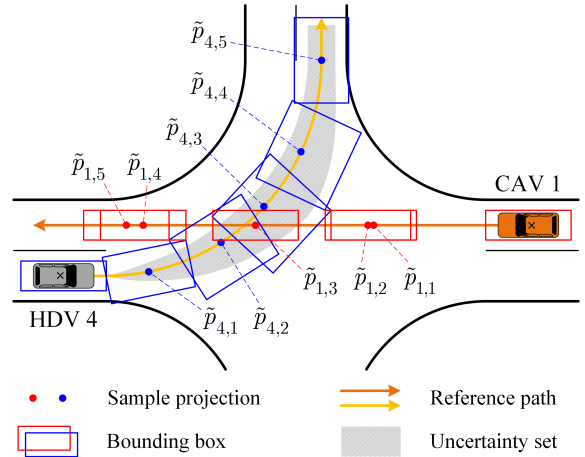


Fig. 4. Illustration of the traffic conflict between CAV 1 and HDV 4 in Fig. 2. The path uncertainty of HDV 4 is reflected in its bounding box, which becomes wider as the path uncertainty increases.

It should be noted that the collision avoidance constraints (27) are able to handle crossing, following, merging, and diverging conflicts involving CAVs in a unified linear form; however, conflicts between HDVs are not included as they cannot be directly resolved through the coordinated control

of CAVs. This exclusion is handled by the notation $\{i, j\} \not\subseteq \mathcal{N} \setminus \mathcal{M}$ in (27).

D. Problem Reformulation

In the spatial domain, for a given vehicle crossing order $O \in \mathcal{N}^N$, the coordinated control problem for CAVs is now reformulated as

$$\min_{\tilde{\mathbf{u}}_C, \boldsymbol{\lambda}} J(\boldsymbol{\lambda}) + \sum_{i=1}^M \tilde{J}_i(\tilde{\mathbf{x}}_i(p), \tilde{u}_i(p), \tilde{u}'_i(p)) \quad (29a)$$

subject to

$$\tilde{\mathbf{x}}'_i(p) = A\tilde{\mathbf{x}}_i(p) + B\tilde{u}_i(p), \quad \forall i \in \mathcal{M}, \quad (29b)$$

$$\tilde{\mathbf{x}}_i(p) \in [\tilde{\mathbf{x}}_i^{\min}(p), \tilde{\mathbf{x}}_i^{\max}(p)], \quad \forall i \in \mathcal{M}, \quad (29c)$$

$$\tilde{u}_i(p) \in z_i^3(p) [-a_i^{\max}, -a_i^{\min}], \quad \forall i \in \mathcal{M}, \quad (29d)$$

$$t_{ij}(\tilde{p}_{\text{out}}, \tilde{p}_{\text{in}}) + \lambda_{ij}(\tilde{p}_{\text{in}}) \leq -t_j^{\text{des}}, \quad \lambda_{ij}(\tilde{p}_{\text{in}}) \in [-t_j^{\text{des}}, 0], \\ \forall (\tilde{p}_{\text{out}}, \tilde{p}_{\text{in}}) \in \mathcal{C}_{ij}, \quad \forall i, j \in \mathcal{N}, \quad \{i, j\} \not\subseteq \mathcal{N} \setminus \mathcal{M}, \quad (29e)$$

$$\tilde{\mathbf{x}}_i(p_{i0}) = \tilde{\mathbf{x}}_{i0}, \quad \forall i \in \mathcal{M}, \quad (29f)$$

where the constraints (29b)-(29d) are imposed for all $p \in [p_{i0}, p_{if}]$, and $\boldsymbol{\lambda}$ is a vector consisting of all the slack variables, which together with the control signals of all CAVs, $\tilde{\mathbf{u}}_C = [\tilde{u}_1(p) \dots \tilde{u}_M(p)]$, serve as the optimization variables. Assuming that the objective function in (29a) is nonlinear, problem (29) is a nonconvex NLP, and the nonconvexity stems from the control constraints (29d). Except for these, all other constraints are linear. The NLP (29) can be solved iteratively using linearized convex subproblems, a solution method commonly referred to as sequential convex programming (SCP), or sequential quadratic programming (SQP) if the subproblems are QPs (both convex and nonconvex). To ensure applicability in dynamic mixed traffic with uncertainty, program (29) is deployed in the MPC framework, see the following section.

IV. CENTRALIZED MODEL PREDICTIVE CONTROL AND COMPUTATIONALLY EFFICIENT SOLUTIONS

In this section, the coordinated control problem (29) is discretized and written in a receding horizon fashion, convex quadratic cost functions are formulated, and an RTI scheme is developed using the inner approximation of the search space to improve computational efficiency.

A. Receding Horizon Optimization

In order to compensate for motion prediction deviations for HDVs and other possible disturbances, it is necessary to iteratively update and resolve the coordinated control problem. For each CAV $i \in \mathcal{M}$, let $\mathcal{P}_i = \{p_{i0}, p_{i0} + \Delta p, \dots, p_{if} + \epsilon_i\}$ denote the set of its discrete distance samples corresponding to the continuous sample interval $[p_{i0}, p_{if}]$, where Δp is the distance sampling interval and $\epsilon_i \in [0, \Delta p)$ is a relaxation term introduced to guarantee uniform sampling. Let k be

the discrete sampling variable. Then, the coordinated control problem (29) is discretized as

$$\min_{\tilde{\mathbf{u}}_C, \boldsymbol{\lambda}^d} J^d(\boldsymbol{\lambda}^d) + \sum_{i=1}^M \tilde{J}_i^d(\tilde{\mathbf{x}}_i(k), \tilde{u}_i(k)) \quad (30a)$$

subject to

$$\tilde{\mathbf{x}}_i(k + \Delta p) = A^d \tilde{\mathbf{x}}_i(k) + B^d \tilde{u}_i(k), \quad \forall i \in \mathcal{M}, \quad (30b)$$

$$\tilde{\mathbf{x}}_i(k) \in [\tilde{\mathbf{x}}_i^{\min}(k), \tilde{\mathbf{x}}_i^{\max}(k)], \quad \forall i \in \mathcal{M}, \quad (30c)$$

$$\tilde{u}_i(k) \in z_i^3(k) [-a_i^{\max}, -a_i^{\min}], \quad \forall i \in \mathcal{M}, \quad (30d)$$

$$t_{ij}(\tilde{k}_{\text{out}}, \tilde{k}_{\text{in}}) + \lambda_{ij}(\tilde{k}_{\text{in}}) \leq -t_j^{\text{des}}, \quad \lambda_{ij}(\tilde{k}_{\text{in}}) \in [-t_j^{\text{des}}, 0], \\ \forall (\tilde{k}_{\text{out}}, \tilde{k}_{\text{in}}) \in \mathcal{C}_{ij}^d, \quad \forall i, j \in \mathcal{N}, \quad \{i, j\} \not\subseteq \mathcal{N} \setminus \mathcal{M}, \quad (30e)$$

$$\tilde{\mathbf{x}}_i(p_{i0}) = \tilde{\mathbf{x}}_{i0}, \quad \forall i \in \mathcal{M}, \quad (30f)$$

where the constraints (30b) and (30d) hold for all $k \in \mathcal{P}_i^- = \mathcal{P}_i \setminus \{p_{if} + \epsilon_i\}$, the constraints (30c) hold for all $k \in \mathcal{P}_i$, the superscript $(\cdot)^d$ denotes the discretized version, and

$$A^d = \begin{bmatrix} 1 & \Delta p \\ 0 & 1 \end{bmatrix}, \quad B^d = \begin{bmatrix} \frac{\Delta p^2}{2} & \Delta p \end{bmatrix}^\top. \quad (31)$$

Assume that all CAVs have synchronized clocks. After solving the discretized problem (30) each time, each CAV $i \in \mathcal{M}$ implements the first part $\{\tilde{u}_i^*(p_{i0}), \dots, \tilde{u}_i^*(p_{i0} + (n_i - 1)\Delta p)\}$ of its optimal control sequence over a pre-specified time sampling period Δt , where n_i is the number of control steps for CAV i , given as $n_i = \max\{n \in \{1, \dots, |\mathcal{P}_i^-|\} \mid t_i^*(p_{i0} + (n - 1)\Delta p) < \Delta t\}$. Then, problem (30) is updated based on the new traffic state and crossing order (if any), and is re-solved over the shifted horizon.

Note that the proposed centralized MPC is iterated with the time sampling period Δt but solved in the spatial domain, so the number of control steps may be different for the same CAV at different iterations and for different CAVs at the same iteration. In addition, the control horizon for each CAV is shrinking as the number of MPC iterations increases, indicating that the computational load of the MPC algorithm is decreasing as CAVs are approaching their final positions and increasing as new CAVs enter the intersection.

B. Convex Quadratic Cost Functions

Speed tracking and travel time reduction are commonly used cost functions for the temporal domain problem (10), and their convex quadratic formulations for the spatial domain problem (30) are provided here.

1) *Speed Tracking*: The reference speed is tracked using the cost function

$$\tilde{J}_{i1}^d(\cdot) = \tilde{J}_{i1}^d(\tilde{\mathbf{x}}_i(k), \tilde{u}_i(k)) + \tilde{J}_{i2}^d(\tilde{\mathbf{x}}_i(k), \tilde{u}_i(k)), \quad (32)$$

where $\tilde{J}_{i1}^d(\cdot)$ and $\tilde{J}_{i2}^d(\cdot)$ represent the costs of being within and beyond the actual finite prediction horizon, respectively, thus effectively mimicking an infinite horizon. Specifically,

$$\tilde{J}_{i1}^d(\cdot) = q_{i1}(z_i(p_{if} + \epsilon_i) - 1/v_{ir}(p_{if} + \epsilon_i))^2 \\ + \sum_{k \in \mathcal{P}_i^-} [q_{i1}(z_i(k) - 1/v_{ir}(k))^2 + r_i \tilde{u}_i^2(k) \\ + e_i(\tilde{u}_i(k) - \tilde{u}_i(k - \Delta p))^2], \quad (33)$$

where $v_{ir}(\cdot)$ is the reference speed and q_{i1} , r_i , and e_i are positive weights. Penalties for the control signal and its difference are included to mitigate sudden shifts in acceleration and jerk, thus reducing discomfort and energy consumption. The cost after the actual finite prediction horizon and towards infinity is formulated as

$$\tilde{J}_{i2}^d(\cdot) = \sum_{k \in \mathcal{P}_i^+} [q_{i1}(z_i(k) - 1/v_{ir,s})^2 + r_i \tilde{u}_i^2(k)], \quad (34)$$

where $\mathcal{P}_i^+ = \{p_{if} + \epsilon_i, p_{if} + \epsilon_i + \Delta p, \dots, \infty\}$ and $v_{ir,s}$ is the steady state reference speed. This cost is introduced to stabilize the second state of the system, $z_i(k)$. In the standard linear-quadratic regulator fashion, it can be shown that

$$\tilde{J}_{i2}^d(\cdot) = P_i(z_i(p_{if}) - 1/v_{ir,s})^2, \quad (35)$$

where

$$P_i = \frac{q_{i1}}{2} + \sqrt{\left(\frac{q_{i1}}{2}\right)^2 + \frac{q_{i1}r_i}{\Delta p^2}}$$

is the solution to the discrete algebraic Riccati equation.

2) *Travel Time Reduction*: The final travel time is minimized using the cost function

$$\tilde{J}_i^d(\cdot) = q_{i2}t_i(p_{if} + \epsilon_i) + \sum_{k \in \mathcal{P}_i^-} [r_i \tilde{u}_i^2(k) + e_i(\tilde{u}_i(k) - \tilde{u}_i(k - \Delta p))^2], \quad (36)$$

where q_{i2} is a positive weight and the summation term is a penalty for discomfort and energy consumption. At the traffic control level, this cost is often used to maximize throughput.

3) *Penalties for Slack Variables*: The cost of exploiting the slack variables is formulated as

$$J^d(\boldsymbol{\lambda}^d) = N_s q_s \|\boldsymbol{\lambda}^d\|^2, \quad (37)$$

where N_s is the number of the discretized slack variables and q_s is a large positive weight.

C. Real-Time Iteration

Although the NLP (30) can be solved with an off-the-shelf solver, this might be time-consuming if the solver has to run until convergence. A computationally efficient solution is to stop the SCP/SQP scheme after only one iteration in each MPC update, which is known as RTI. In order to apply RTI, we need to ensure that the feasible solution to the first subproblem of the SCP/SQP scheme always yields a feasible solution to the original problem (even when the slack variables are not used).

Recalling the continuous control constraints (29d), it is found that the lower bound is convex and the upper bound is concave. Therefore, the linearization of the control constraints (29d) is an inner approximation to the original search space, which means that feasible points within the linearized bounds are also feasible in the original nonconvex set. Using a first-order Taylor expansion, the constraints (29d) are linearized around the lethargy $z_{i,\text{lin}}(p)$, which is then discretized to yield

$$\tilde{u}_i(k) \in [\tilde{u}_i^{\min}(k, z_i(k)), \tilde{u}_i^{\max}(k, z_i(k))], \quad \forall i \in \mathcal{M}, \quad (38)$$

with

$$\begin{aligned} \tilde{u}_i^{\min}(k, z_i(k)) &= a_i^{\max}(2z_{i,\text{lin}}(k) - 3z_i(k))z_{i,\text{lin}}^2(k), \\ \tilde{u}_i^{\max}(k, z_i(k)) &= a_i^{\min}(2z_{i,\text{lin}}(k) - 3z_i(k))z_{i,\text{lin}}^2(k). \end{aligned} \quad (39)$$

Now, by replacing the nonconvex constraints (30d) in the original problem (30) with linear constraints (38), the target subproblem is obtained, which is a computationally efficient convex QP. This allows the application of RTI.

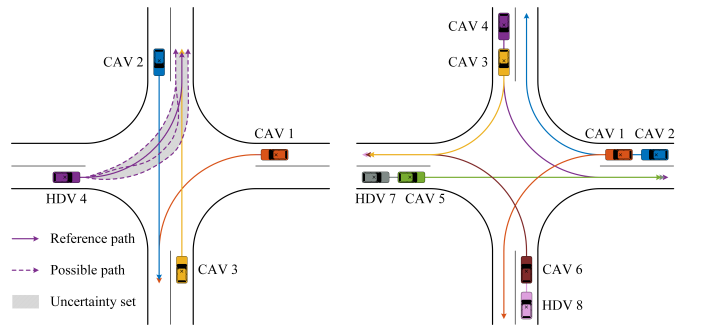
It should be noted that in the first MPC iteration for each CAV $i \in \mathcal{M}$, since there is no previous solution available, the inverse of the reference and maximum speeds are chosen to linearize the control constraints for the speed tracking cost and the travel time reduction cost, respectively. Thereafter, for both cost functions, the linearization is performed about the previous solution, shifted by n_i samples.

V. SIMULATION RESULTS

In this section, the proposed MPC is validated on the scenarios shown in Fig. 5, where the lane width is 4 m, the central area is 30 m across, and the control boundary is a circle with a radius of 90 m, whose center coincides with the center of the central area. The path speed limit is $v_l^s(p) \equiv 50$ km/h for all $l \in \mathcal{L}$. For each CAV $i \in \mathcal{M}$, the longitudinal acceleration limits are $a_i^{\min} = -3.5$ m/s² and $a_i^{\max} = 2$ m/s², the maximum acceptable centripetal acceleration is $a_{in}^{\max} = 2$ m/s², and the maximum speed is

$$v_i^{\max}(p) = \begin{cases} 50 \text{ km/h}, & \text{if } \kappa_i(p) = 0, \\ 21.0 \text{ km/h}, & \text{if } \kappa_i(p) = 0.0588, \\ 18.4 \text{ km/h}, & \text{if } \kappa_i(p) = 0.0769, \end{cases} \quad (40)$$

where the curvature $\kappa_i(p) = 0$ corresponds to going straight, $\kappa_i(p) = 0.0588$ corresponds to turning left, and $\kappa_i(p) = 0.0769$ corresponds to turning right. The desired time gap is set to $t_j^{\text{des}} = 1.1$ s for all $j \in \mathcal{N}$. The distance sampling interval is chosen to be $\Delta p = 1$ m. The time sampling period is chosen to be $\Delta t = 0.5$ s.



(a) Scenario 1: Four vehicles consisting of 3 CAVs and 1 HDV traveling through an unsignalized intersection. (b) Scenario 2: Eight vehicles consisting of 6 CAVs and 2 HDVs traveling through an unsignalized intersection.

Fig. 5. Scenarios investigated in the case study.

The two cost functions presented in Section IV-B, speed tracking and travel time reduction, are used in the case study with the weights

$$q_{i1} = \frac{w_{i1}\Delta p}{z_{im}^3}, \quad r_i = \frac{w_{i2}\Delta p}{z_{im}^5}, \quad e_i = \frac{w_{i3}}{\Delta p z_{im}^7}, \quad q_{i2} = 500, \quad (41)$$

where $w_{i1} = 1$, $w_{i2} = 1$, and $w_{i3} = 0.5$ are the weights corresponding to the temporal domain problem (10), as detailed in [27], and z_{im} is the mean value of the linearization lethargy $z_{i,\text{lin}}(k)$. In addition, the weight for penalizing the slack variables is $q_s = 10000$.

The proposed MPC is implemented in MATLAB and the coordinated control problem (30) is solved by applying RTI and using the optimization tool CasADi. All simulations are performed on a laptop with an Intel Core i9-13900HX CPU at 2.20 GHz and 32 GB RAM.

The simulation results are divided into three parts: the effect of motion uncertainty, the comparison of cost functions, and the analysis of computational effort and optimality.

TABLE I
SPECIFIC VEHICLE PARAMETERS FOR SCENARIO 1 AND SCENARIO 2

Description	Values
Initial position (m)	[10 15 20 25]
Initial speed (km/h)	[25 10 30 0 20 30 5 15]
Initial acceleration (m/s ²)	[40 42 44 46]
Reference speed (km/h)	[34 32 42 40 38 46 36 44]
Crossing order	[0 0 0 0 0 0 - -]
	[40 42 44 -]
	[50 50 50 50 50 50 - -]
	[4 2 3 1]
	[3 6 8 1 2 5 7 4]

A. Effect of Motion Uncertainty

In this part, the proposed algorithm is applied to Scenario 1, a typical mixed-traffic unsignalized intersection scenario containing both side and rear-end conflicts between CAVs and between CAVs and HDVs, as depicted in Fig. 5(a). The exact path of HDV 4 turning left is unknown and is assumed to be contained within the uncertainty set shown in the shaded area. To investigate the effect of motion uncertainty, 100 cases with varying paths for HDV 4 are designed and the same hypothetical speed trajectory is assigned to HDV 4 in all cases for comparison. The initial conditions of the vehicles are listed in Table I. The speed tracking cost is chosen as the cost function.

The solution of the first MPC iteration is plotted in Fig. 6, which is the same for all 100 cases. The shaded area reflects the speed uncertainty of HDV 4, within which the actual trajectory of HDV 4 is contained, and the upper and lower boundaries are the predicted trajectories with the minimum and maximum travel times, respectively. Since HDV 4 is designated to pass first, the predicted trajectory with the maximum travel time is adopted for robust collision avoidance. For each vehicle pair at risk of collision, the critical zone corresponding to its minimum time gap is labeled by a pair of triangles with the same number. The physical meaning of the time gap for a vehicle pair is the time difference between the follower entering the critical zone and the leader exiting it. It turns out that all the minimum time gaps are equal to

or greater than the desired value of 1.1 s, indicating that the solution fulfills the unrelaxed collision avoidance constraints even in the worst case. Indeed, this property is also present in each subsequent MPC iteration. Furthermore, for visual presentation, the spatial-temporal diagram between the dashed lines in Fig. 6 is shown in Fig. 7, from which it is evident that the trajectories of all vehicles do not intersect and leave a safety margin.

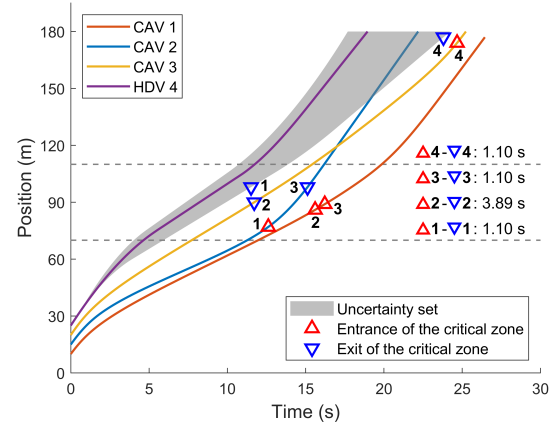


Fig. 6. Solution of the first MPC iteration for Scenario 1. The purple line indicates the actual trajectory of HDV 4, which is contained within the uncertainty set depicted by the shaded area. For each vehicle pair at risk of collision, the critical zone corresponding to its minimum time gap is labeled by a pair of triangles with the same number.

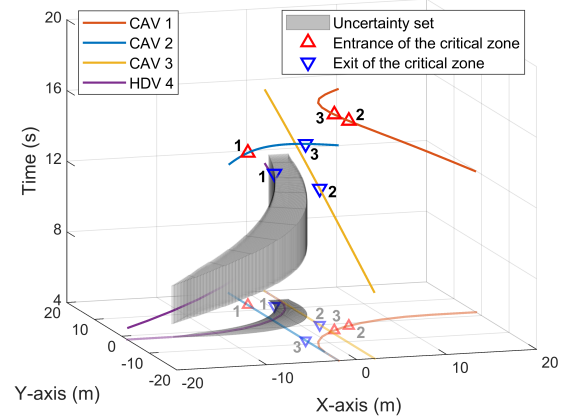


Fig. 7. Local spatio-temporal diagram derived from the first MPC iteration for Scenario 1, corresponding to the portion between the dashed lines in Fig. 6. The shaded space shows the motion uncertainty of HDV 4, where the X-Y projection plane reflects the path uncertainty and the height reflects the speed uncertainty. The trajectories of all vehicles do not intersect and leave a safety margin, indicating that the solution is collision-free even in the worst case.

The trajectory results of coordinated control for the 100 cases are presented in Fig. 8. HDV 4 is assumed to experience uniform deceleration, uniform speed, variable acceleration, and uniform speed in sequence, as shown by the purple speed profile. The three CAVs first slow down to avoid a collision in the central area and later accelerate to their respective reference speeds while ensuring safety. It can be seen that the

solutions for the different cases do not differ much and are all smooth. This is because the motion uncertainty of HDV 4 is updated and imposed in each MPC iteration, allowing the CAVs to have enough room for error to adapt to the real situation with only minor control adjustments. To confirm that the solutions are collision-free, box plots are used to show the minimum time gaps for vehicle pairs with collision risk, as depicted in Fig. 9. Since all of them are equal to or greater than the desired time gap of 1.1 s, the solutions for all cases fulfill the unrelaxed collision avoidance constraints.

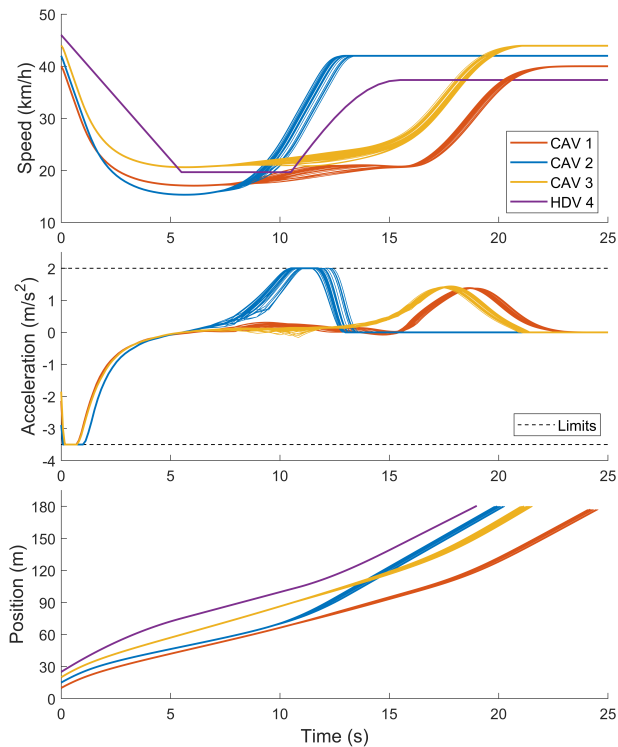


Fig. 8. Trajectory results of coordinated control for the 100 cases of Scenario 1. Each CAV fulfills the speed and acceleration limits in all cases.

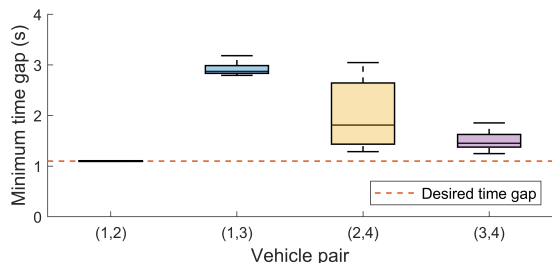


Fig. 9. Minimum time gaps for vehicle pairs with collision risk for the 100 cases of Scenario 1.

Further from Fig. 9, the minimum time gap between CAV 1 and CAV 2 is consistently 1.1 s across the different cases, compared to 1.29 s to 3.05 s between CAV 2 and HDV 4, and 1.25 s to 1.86 s between CAV 3 and HDV 4. This suggests that the motion uncertainty of HDV 4 leads to varying degrees of conservative solutions, somewhat affecting the time efficiency of the CAVs. To visualize this feature, three representative cases are selected for comparison, corresponding in turn to

HDV 4 traveling along the reference path, along the counterclockwise boundary of the uncertainty set, and along the clockwise boundary of the uncertainty set, and the snapshots when CAV 2 is about to get rid of the risk of collision with HDV 4 are shown in Fig. 10. Moreover, the minimum time gaps for vehicle pairs with collision risk are listed in Table II. It can be observed that for CAV 2, the solution in Case 2 is the most time-efficient. This is because the collision location in Case 2 is the closest for CAV 2, which constitutes a worst-case scenario, covered by the collision avoidance constraints and plays a decisive role. Accordingly, for the other two cases, more conservative solutions are produced. Nevertheless, these efficiency losses are acceptable given the priority of safety. A similar phenomenon is seen for CAV 3, for which the solution in Case 3 is the most time-efficient, while the solution for CAV 1 is indirectly affected by the motion uncertainty of HDV 4. The conservatism in robust optimization can be reduced by exploiting the distributional characteristics of uncertainty parameters. However, this involves data-driven feature extraction of driving behavior, which is beyond the scope of this paper, and we leave it for future work.

TABLE II
MINIMUM TIME GAPS FOR VEHICLE PAIRS WITH COLLISION RISK FOR THE THREE SELECTED CASES

	Case 1	Case 2	Case 3
$t_1 - t_2$	1.10 s	1.10 s	1.10 s
$t_1 - t_3$	2.89 s	2.80 s	2.88 s
$t_2 - t_4$	1.91 s	1.29 s	2.92 s
$t_3 - t_4$	1.64 s	1.86 s	1.31 s

Note that when the uncertainty set is not given or fails, the proposed MPC may still work by making initial guesses about the HDV in question, e.g., assuming its speed is constant, assuming it is traveling along a certain feasible path. However, in that case the robustness of collision avoidance is no longer guaranteed and the trajectory smoothness becomes susceptible. In addition, there will inevitably be situations where HDVs do not follow the scheduled crossing order, which requires intent recognition to adjust the crossing order in time. This important consideration is left for future work.

B. Comparison of Cost Functions

In this part, the proposed algorithm is applied to Scenario 2, where there are two vehicles in each of the four entry lanes, as depicted in Fig. 5(b). Scenario 2 comprehensively covers the four types of vehicle conflict situations at unsignalized intersections: crossing, following, merging, and diverging. The motions of HDV 7 and HDV 8 are simulated using the constant time gap car-following law

$$u_i(t) = c_1(d_i(t) - d_0 - Tv_i(t)) + c_2(v_{i1}(t) - v_i(t)), \quad (42)$$

where c_1 and c_2 are feedback gains, $d_i(t)$ is the spacing between HDV i and its leader, d_0 is the spacing margin, T is the target time gap, and $v_i(t)$ and $v_{i1}(t)$ are the speeds of HDV i and its leader, respectively. Referring to [42] and [43],

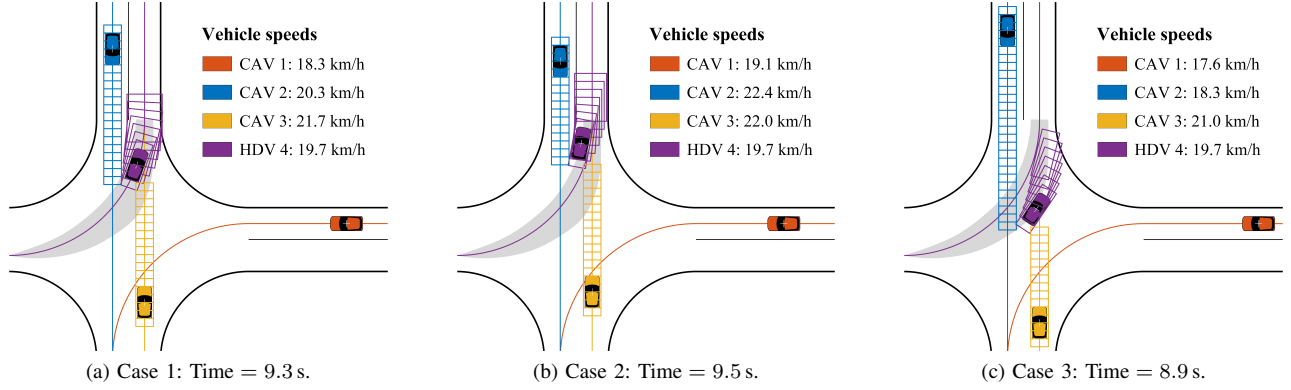


Fig. 10. Snapshots when CAV 2 is about to get rid of the risk of collision with HDV 4 for the three selected cases. The bounding box of HDV 4 shows its potential path offset at the spatial sample.

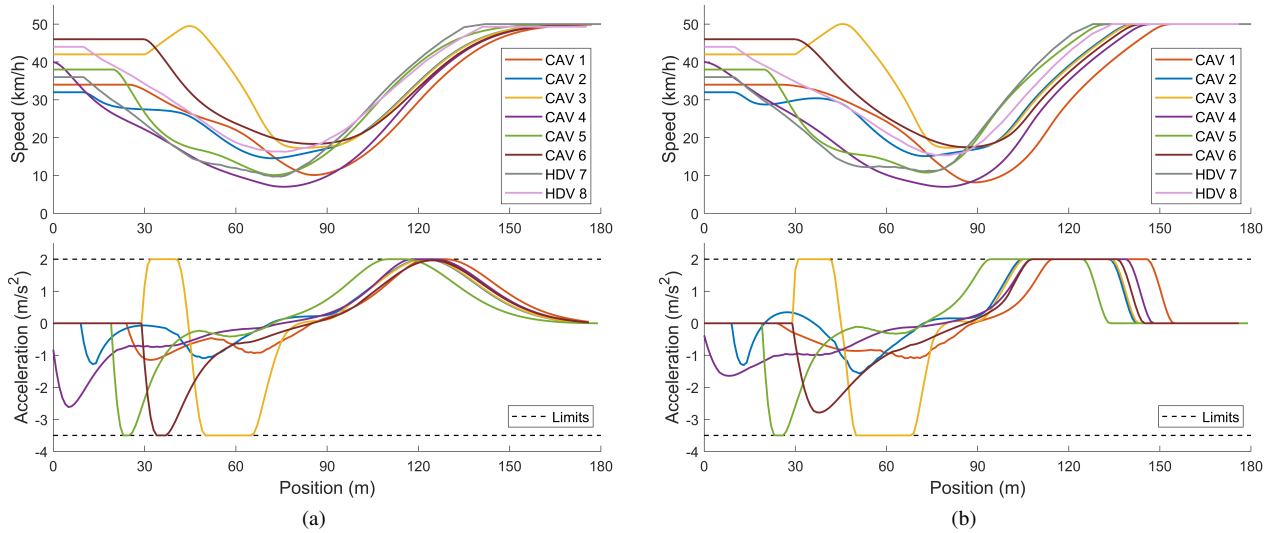


Fig. 11. Trajectory results of coordinated control for Scenario 2: (a) using the speed tracking cost; (b) using the travel time reduction cost. All CAVs fulfill the speed and acceleration limits under both costs.

$c_1 = 0.23$, $c_2 = 0.07$, $d_0 = 2$ m, and $T = 1.4$ s are taken. The initial conditions of the vehicles are listed in Table I.

The trajectory results using the speed tracking cost and the travel time reduction cost are presented in Fig. 11. To determine that the solutions are collision-free, the time gaps for vehicle pairs at risk of collision are shown in Fig. 12, where the curves indicate the time gaps for vehicle pairs with overlapping paths, and the crosses indicate the minimum time gaps for vehicle pairs with intersecting paths. Since all of them are greater than zero, the solutions obtained with both costs are collision-free. Moreover, the time gap between CAV 6 and HDV 8 is observed to be less than the desired value of 1.1 s early on (see the pink curves labeled $t_8 - t_6$), suggesting that the relaxed collision avoidance constraints are activated to allow for moderate violations of the original hard constraints, thus effectively adapting to the aggressive following behavior of HDVs.

Although both costs are feasible, there are some differences in the solutions produced. As seen in Fig. 11, the travel time reduction cost is more sensitive to speed loss, evident in the

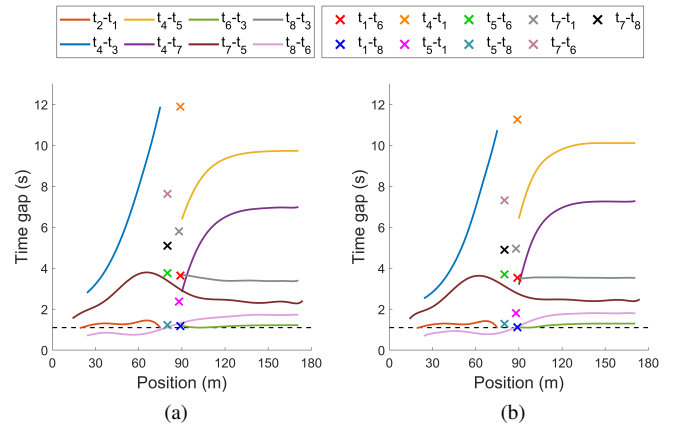


Fig. 12. Time gaps for vehicle pairs at risk of collision in Scenario 2: (a) using the speed tracking cost; (b) using the travel time reduction cost. The curves indicate the time gaps for vehicle pairs with overlapping paths, and the crosses indicate the minimum time gaps for vehicle pairs with intersecting paths. The black dashed lines mark the desired time gap of 1.1 s.

TABLE III
PERFORMANCE MEASURES OF DIFFERENT SOLUTION SCHEMES FOR CONTROL HORIZONS OF 50 TO 600 SAMPLES

	STC		RTI (one iteration)	
	Min/Max Comp. time (s)	Min/Max No. of iterations	Min/Max Comp. time (s)	Min/Max Sol. deviation (%)
Speed tracking cost	0.513/326.264	20/45	0.005/3.616	< 0.01/2.26
Travel time reduction cost	0.581/381.758	23/69	0.006/4.187	< 0.01/1.18

fact that the CAVs accelerate faster after passing through the central area and reach the path speed limit of 50 km/h in a shorter distance, whereas the speed tracking cost yields smoother trajectories at this stage. As expected, the sum of the final travel times of the CAVs is less under the time cost, 137.2s, compared to 141.5s under the speed cost, while the final travel times of the last vehicle (CAV 4) are 34.1s and 35.3s, respectively. Therefore, the travel time reduction cost motivates CAVs to cross the intersection faster than the speed tracking cost.

C. Analysis of Computational Effort and Optimality

In this part, the computational effort and optimality of the proposed RTI scheme are examined on Scenario 2, for which the original NLP is solved to convergence (this scheme is referred to as STC) for comparison. Specifically, RTI and STC are implemented utilizing the solvers OSQP and IPOPT, respectively. The computation times of the two solution schemes with respect to the control horizon are shown in Fig. 13, and the performance measures are summarized in Table III. It can be seen that, all else being equal, RTI solves significantly faster than STC, by a factor of 111 on average, and that the computational effort with the speed tracking cost is slightly lower than that with the travel time reduction cost. Further, Fig. 14 shows the deviation of the solution obtained by RTI from the optimum produced by STC, and it turns out that the solution deviation is less than 2.26% for different control horizons and cost functions, indicating that RTI yields a near-optimal solution. Thus, the proposed RTI scheme achieves a good trade-off between computational effort and optimality.

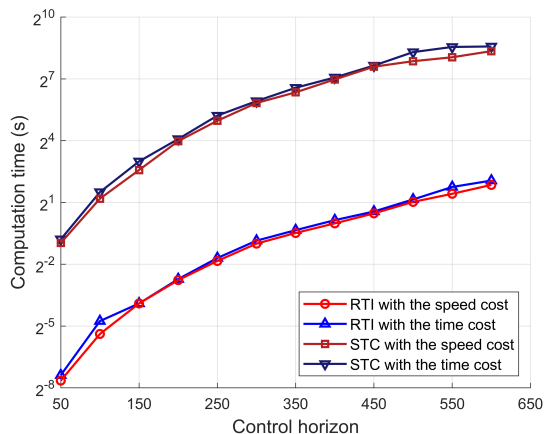


Fig. 13. Computation time of different solution schemes with respect to the control horizon.

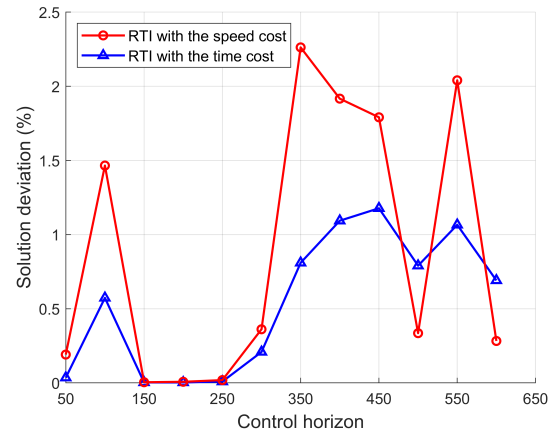


Fig. 14. Deviation of the solution obtained by RTI from the optimum produced by STC against the control horizon.

It should be noted that the computational effort of the proposed algorithm grows super-linearly as the control horizon is extended, a drawback that is difficult to address in a centralized control architecture. An effective way to reduce the computational effort is dynamic sampling, i.e., the distance sampling interval increases with vehicle speed, thereby shortening the control horizon. On the other hand, since the actual computation time also depends on hardware and software, the computational efficiency can be further improved by implementing RTI on a dedicated platform, especially given that the formulated subproblem is a convex QP. Therefore, the proposed algorithm is considered to have good potential for real-time applications in limited-scale scenarios.

VI. CONCLUSION AND FUTURE WORK

This paper proposes a coordinated centralized MPC for trajectory planning of CAVs at an unsignalized intersection in mixed traffic. By sampling in distance and using an exact change of variables, the coordinated control problem is formulated as an NLP in the spatial domain. This approach provides simplicity in terms of: 1) handling crossing, following, merging, and diverging vehicle conflicts with unified linear collision avoidance constraints; 2) handling spatially varying speed limits with linear state constraints; and 3) requiring no additional steps to anchor the control horizon. The motion uncertainty of HDVs is modeled at both path and speed levels, based on which the robustness of collision avoidance is ensured in both spatial and temporal dimensions. The subproblem of the NLP is formulated as a convex QP

using the inner approximation of the solution space, thus enabling the application of RTI for efficient implementation of MPC. The efficacy, robustness, and potential for real-time applications of the proposed method are demonstrated through simulation case studies. The results show that the proposed control scheme provides collision-free and smooth trajectories with state and control constraints satisfied, and achieves a good trade-off between computational effort and optimality. It is worth mentioning that the proposed method is also applicable to a wider range of right-of-way conflict scenarios, such as roundabouts and ramp merging/diverging.

Future work includes crossing scheduling for unsignalized intersections in mixed traffic. One challenge is to cope with the intent uncertainty of HDVs, determine the right-of-way priority of CAVs with respect to HDVs, and derive a feasible scheduling decision space. Another challenge is to balance the overall computational effort and optimality to achieve efficient cooperative driving that integrates crossing scheduling and trajectory planning. In addition, investigating distributed MPC to enhance the real-time performance of coordinated control is also a research direction worth exploring.

APPENDIX A

PATH UNCERTAINTY SET MODELING

For each HDV $i \in \mathcal{N} \setminus \mathcal{M}$, its path uncertainty set is written as $\mathcal{U}_i(\tilde{p}) = [\xi_i^{\min}(\tilde{p}), \xi_i^{\max}(\tilde{p})]$, where $\tilde{p} \in [\tilde{p}_{i0}, \tilde{p}_{i\bar{r}}]$. The bounds of the path uncertainty set are modeled as

$$\begin{aligned}\xi_i^{\min}(\tilde{p}) &= \max \{ \xi_{ir}^{\min}(\tilde{p}), \min \bar{\xi}_i(\tilde{p}) \}, \\ \xi_i^{\max}(\tilde{p}) &= \min \{ \xi_{ir}^{\max}(\tilde{p}), \max \bar{\xi}_i(\tilde{p}) \},\end{aligned}\quad (43)$$

where the physical limits, $\xi_{ir}^{\min}(\tilde{p}) \leq 0$ and $\xi_{ir}^{\max}(\tilde{p}) \geq 0$, are preset based on the road geometry, and

$$\begin{aligned}\bar{\xi}_i(\tilde{p}) &= \xi_i(\tilde{p}_{i0}) + \int_{\tilde{p}_{i0}}^{\tilde{p}} \tan \theta_i(\tilde{s}) d\tilde{s}, \\ \theta_i(\tilde{p}) &\in [\theta_i^{\min}(\tilde{p}), \theta_i^{\max}(\tilde{p})].\end{aligned}\quad (44)$$

Here, $\xi_i(\tilde{p}_{i0})$ is the initial offset of HDV i , \tilde{s} is the integral variable corresponding to the projection variable \tilde{p} , and $\theta_i(\tilde{p})$ is the yaw angle of HDV i with respect to the reference path, with the limits $\theta_i^{\min}(\tilde{p}) \leq 0$ and $\theta_i^{\max}(\tilde{p}) \geq 0$.

Given the path uncertainty set, any possible path of HDV i can be described by the parametric equations

$$\begin{aligned}x_i(\tilde{p}, \xi_i(\tilde{p})) &= x_{ir}(\tilde{p}) - \xi_i(\tilde{p}) \cdot \sin \psi_{ir}(\tilde{p}), \\ y_i(\tilde{p}, \xi_i(\tilde{p})) &= y_{ir}(\tilde{p}) + \xi_i(\tilde{p}) \cdot \cos \psi_{ir}(\tilde{p}),\end{aligned}\quad (45)$$

where $\tilde{p} \in [\tilde{p}_{i0}, \tilde{p}_{i\bar{r}}]$, $\xi_i(\tilde{p}) \in \mathcal{U}_i(\tilde{p})$, and $x_i(\tilde{p}, \xi_i(\tilde{p}))$, $y_i(\tilde{p}, \xi_i(\tilde{p}))$ are the global coordinates of HDV i with projection \tilde{p} and offset $\xi_i(\tilde{p})$.

REFERENCES

- [1] A. Matin and H. Dia, "Impacts of connected and automated vehicles on road safety and efficiency: A systematic literature review," *IEEE Trans. Intell. Transp. Syst.*, vol. 24, no. 3, pp. 2705–2736, 2023. DOI: 10.1109/TITS.2022.3227176
- [2] M. M. Rahman and J.-C. Thill, "Impacts of connected and autonomous vehicles on urban transportation and environment: A comprehensive review," *Sustain Cities Soc.*, vol. 96, p. 104649, 2023. DOI: 10.1016/j.scs.2023.104649
- [3] Z. Zhang, H. Liu, M. Lei, X. Yan, M. Wang, and J. Hu, "Review on the impacts of cooperative automated driving on transportation and environment," *Transp. Res. Part D Transp. Environ.*, vol. 115, p. 103607, 2023. DOI: 10.1016/j.trd.2023.103607
- [4] Y. Ji, Z. Zhou, Z. Yang, Y. Huang, Y. Zhang, W. Zhang, et al., "Toward autonomous vehicles: A survey on cooperative vehicle-infrastructure system," *iScience*, vol. 27, no. 5, p. 109751, Apr. 17 2024. DOI: 10.1016/j.isci.2024.109751
- [5] N. Zhang, W.-B. Zhang, J. Li, and K. Zhang, "Unsignalized intersections: Can ITS offer improved efficiency and safety?" in 2011 14th International IEEE Conference on Intelligent Transportation Systems (ITSC), IEEE, 2011, pp. 1948–1953. DOI: 10.1109/ITSC.2011.6083152
- [6] S. M. Mousavi, O. A. Osman, D. Lord, K. K. Dixon, and B. Dadashova, "Investigating the safety and operational benefits of mixed traffic environments with different automated vehicle market penetration rates in the proximity of a driveway on an urban arterial," *Accid. Anal. Prev.*, vol. 152, p. 105982, Mar. 2021. DOI: 10.1016/j.aap.2021.105982
- [7] S. Li, J. Zhang, Z. Chen, and L. Li, "Theoretical analysis of cooperative driving at idealized unsignalized intersections," *Tsinghua Sci. Technol.*, vol. 29, no. 1, pp. 257–270, 2024. DOI: 10.26599/TST.2022.9010069
- [8] E. Y. Bejarbaneh, H. Du, and F. Naghdy, "Exploring shared perception and control in cooperative vehicle-intersection systems: A review," *IEEE Transactions on Intelligent Transportation Systems*, vol. 25, no. 11, pp. 15 247–15 272, 2024. DOI: 10.1109/TITS.2024.3432634
- [9] Z. Zhong, M. Nejad, and E. E. Lee, "Autonomous and semiautonomous intersection management: A survey," *IEEE Intell. Transp. Syst. Mag.*, vol. 13, no. 2, pp. 53–70, 2021. DOI: 10.1109/MITS.2020.3014074
- [10] J. Rios-Torres and A. A. Malikopoulos, "A survey on the coordination of connected and automated vehicles at intersections and merging at highway on-ramps," *IEEE Trans. Intell. Transp. Syst.*, vol. 18, no. 5, pp. 1066–1077, 2017. DOI: 10.1109/TITS.2016.2600504
- [11] L. Chen and C. Englund, "Cooperative intersection management: A survey," *IEEE Trans. Intell. Transp. Syst.*, vol. 17, no. 2, pp. 570–586, 2016. DOI: 10.1109/TITS.2015.2471812
- [12] M. A. S. Kamal, J.-i. Imura, T. Hayakawa, A. Ohata, and K. Aihara, "A vehicle-intersection coordination scheme for smooth flows of traffic without using traffic lights," *IEEE Trans. Intell. Transp. Syst.*, vol. 16, no. 3, pp. 1136–1147, 2015. DOI: 10.1109/TITS.2014.2354380
- [13] H. Ahn and A. Colombo, "Abstraction-based safety verification and control of cooperative vehicles at road intersections," *IEEE Trans. Automat. Contr.*, vol. 65, no. 10, pp. 4061–4074, 2020. DOI: 10.1109/TAC.2019.2953213
- [14] J. Luo, T. Zhang, R. Hao, D. Li, C. Chen, Z. Na, et al., "Real-time cooperative vehicle coordination at unsignalized road intersections," *IEEE Trans. Intell. Transp. Syst.*, vol. 24, no. 5, pp. 5390–5405, 2023. DOI: 10.1109/TITS.2023.3243940
- [15] K. Dresner and P. Stone, "A multiagent approach to autonomous intersection management," *J. Artif. Intell. Res.*, vol. 31, pp. 591–656, 2008. DOI: 10.1613/jair.2502
- [16] D. Rey, M. W. Levin, and V. V. Dixit, "Online incentive-compatible mechanisms for traffic intersection auctions," *Eur. J. Oper. Res.*, vol. 293, no. 1, pp. 229–247, 2021. DOI: 10.1016/j.ejor.2020.12.030
- [17] E. R. Müller, R. C. Carlson, and W. Kraus, "Time optimal scheduling of automated vehicle arrivals at urban intersections," in 2016 IEEE 19th International Conference on Intelligent Transportation Systems (ITSC), IEEE, 2016, pp. 1174–1179.
- [18] S. A. Fayazi and A. Vahidi, "Mixed-integer linear programming for optimal scheduling of autonomous vehicle intersection crossing," *IEEE Trans. Intell. Veh.*, vol. 3, no. 3, pp. 287–299, 2018. DOI: 10.1109/TIV.2018.2843163
- [19] H. Xu, Y. Zhang, L. Li, and W. Li, "Cooperative driving at unsignalized intersections using tree search," *IEEE Trans. Intell. Transp. Syst.*, vol. 21, no. 11, pp. 4563–4571, 2020. DOI: 10.1109/TITS.2019.2940641
- [20] J. Luo, T. Zhang, and Q. Zhang, "A computationally efficient bi-level coordination framework for cavs at unsignalized intersections," *IEEE Trans. Vehicular Technol.*, vol. 73, no. 2, pp. 1868–1878, 2024. DOI: 10.1109/TVT.2023.3321335
- [21] A. Lombard, A. Noubli, A. Abbas-Turki, N. Gaud, and S. Galland, "Deep reinforcement learning approach for V2X managed intersections of connected vehicles," *IEEE Trans. Intell. Transp. Syst.*, vol. 24, no. 7, pp. 7178–7189, 2023. DOI: 10.1109/TITS.2023.3253867
- [22] R. Chandra and D. Manocha, "Gameplan: Game-theoretic multi-agent planning with human drivers at intersections, roundabouts, and merging," *IEEE Robot. Autom. Lett.*, vol. 7, no. 2, pp. 2676–2683, 2022. DOI: 10.1109/LRA.2022.3144516
- [23] S. Pruekprasert, X. Zhang, J. Dubut, C. Huang, and M. Kishida, "Decision making for autonomous vehicles at unsignalized intersection in

- presence of malicious vehicles,” in *2019 IEEE Intelligent Transportation Systems Conference (ITSC)*. IEEE, 2019, pp. 2299–2304.
- [24] Y. Zhang and C. G. Cassandras, “Decentralized optimal control of connected automated vehicles at signal-free intersections including comfort-constrained turns and safety guarantees,” *Automatica*, vol. 109, p. 108563, 2019. DOI: 10.1016/j.automatica.2019.108563
- [25] A. A. Malikopoulos, C. G. Cassandras, and Y. J. Zhang, “A decentralized energy-optimal control framework for connected automated vehicles at signal-free intersections,” *Automatica*, vol. 93, pp. 244–256, 2018. DOI: 10.1016/j.automatica.2018.03.056
- [26] R. Hult, M. Zanon, S. Gras, and P. Falcone, “An MIQP-based heuristic for optimal coordination of vehicles at intersections,” in *2018 IEEE Conference on Decision and Control (CDC)*. IEEE, 2018, pp. 2783–2790. DOI: 10.1109/CDC.2018.8618945
- [27] N. Murgovski, G. R. de Campos, and J. Sjöberg, “Convex modeling of conflict resolution at traffic intersections,” in *2015 54th IEEE conference on decision and control (CDC)*. IEEE, 2015, pp. 4708–4713. DOI: 10.1109/CDC.2015.7402953
- [28] J. Karlsson, N. Murgovski, and J. Sjöberg, “Optimal conflict resolution for vehicles with intersecting and overlapping paths,” *IEEE Open J. Intell. Transp. Syst.*, vol. 5, pp. 146–159, 2023. DOI: 10.1109/OJITS.2023.3336533
- [29] G. R. De Campos, P. Falcone, R. Hult, H. Wymeersch, and J. Sjöberg, “Traffic coordination at road intersections: Autonomous decision-making algorithms using model-based heuristics,” *IEEE Intell. Transp. Syst. Mag.*, vol. 9, no. 1, pp. 8–21, 2017. DOI: 10.1109/ITS.2016.2630585
- [30] Y. Bian, S. E. Li, W. Ren, J. Wang, K. Li, and H. X. Liu, “Cooperation of multiple connected vehicles at unsignalized intersections: Distributed observation, optimization, and control,” *IEEE Transactions on Industrial Electronics*, vol. 67, no. 12, pp. 10744–10754, 2020. DOI: 10.1109/TIE.2019.2960757
- [31] X. Pan, B. Chen, L. Dai, S. Timotheou, and S. A. Evangelou, “A hierarchical robust control strategy for decentralized signal-free intersection management,” *IEEE Trans. Control Syst. Technol.*, vol. 31, no. 5, pp. 2011–2026, 2023. DOI: 10.1109/TCST.2023.3291536
- [32] R. Hult, M. Zanon, S. Gros, and P. Falcone, “Optimal coordination of automated vehicles at intersections: Theory and experiments,” *IEEE Trans. Control Syst. Technol.*, vol. 27, no. 6, pp. 2510–2525, 2019. DOI: 10.1109/TCST.2018.2871397
- [33] X. Zhang, B. Wang, Y. Lu, H. Liu, J. Gong, and H. Chen, “A hierarchical multi-vehicle coordinated motion planning method based on interactive spatio-temporal corridors,” *IEEE Trans. Intell. Veh.*, vol. 9, no. 1, pp. 2675–2687, 2024. DOI: 10.1109/TIV.2023.3280898
- [34] X. Gong, B. Wang, and S. Liang, “Collision-free cooperative motion planning and decision-making for connected and automated vehicles at unsignalized intersections,” *IEEE Trans. Syst. Man Cybern. Syst.*, vol. 54, no. 5, pp. 2744–2756, 2024. DOI: 10.1109/TSMC.2023.3346275
- [35] S. Jiang, T. Pan, R. Zhong, C. Chen, X. Li, and S. Wang, “Coordination of mixed platoons and eco-driving strategy for a signal-free intersection,” *IEEE Trans. Intell. Transp. Syst.*, vol. 24, no. 6, pp. 6597–6613, 2023. DOI: 10.1109/TITS.2022.3211934
- [36] M. Faris, P. Falcone, and J. Sjöberg, “Optimization-based coordination of mixed traffic at unsignalized intersections based on platooning strategy,” in *2022 IEEE Intelligent Vehicles Symposium (IV)*. IEEE, 2022, pp. 977–983. DOI: 10.1109/IV51971.2022.9827149
- [37] R. Hult, M. Zanon, S. Gros, and P. Falcone, “A semidistributed interior point algorithm for optimal coordination of automated vehicles at intersections,” *IEEE Trans. Control Syst. Technol.*, vol. 30, no. 5, pp. 1977–1989, 2022. DOI: 10.1109/TCST.2021.3132835
- [38] Z. Yao, H. Jiang, Y. Jiang, and B. Ran, “A two-stage optimization method for schedule and trajectory of cavs at an isolated autonomous intersection,” *IEEE Trans. Intell. Transp. Syst.*, vol. 24, no. 3, pp. 3263–3281, 2023. DOI: 10.1109/TITS.2022.3230682
- [39] W. Zhao, R. Liu, and D. Ngoduy, “A bilevel programming model for autonomous intersection control and trajectory planning,” *Transportmetrica A: Transp. Sci.*, vol. 17, no. 1, pp. 34–58, 2021. DOI: 10.1080/23249935.2018.1563921
- [40] A. Hadjigeorgiou and S. Timotheou, “Real-time optimization of fuel-consumption and travel-time of cavs for cooperative intersection crossing,” *IEEE Trans. Intell. Veh.*, vol. 8, no. 1, pp. 313–329, 2023. DOI: 10.1109/TIV.2022.3158887
- [41] X. Pan, B. Chen, S. Timotheou, and S. A. Evangelou, “A convex optimal control framework for autonomous vehicle intersection crossing,” *IEEE Trans. Intell. Transp. Syst.*, vol. 24, no. 1, pp. 163–177, 2023. DOI: 10.1109/TITS.2022.3211272
- [42] V. Milanés and S. E. Shladover, “Modeling cooperative and autonomous adaptive cruise control dynamic responses using experimental data,” *Transp. Res., Part C Emerg. Technol.*, vol. 48, pp. 285–300, 2014. DOI: 10.1016/j.trc.2014.09.001
- [43] L. Xiao, M. Wang, W. Schakel, and B. van Arem, “Unravelling effects of cooperative adaptive cruise control deactivation on traffic flow characteristics at merging bottlenecks,” *Transp. Res., Part C Emerg. Technol.*, vol. 96, pp. 380–397, 2018. DOI: 10.1016/j.trc.2018.10.008



Tong Zhao received the B.S. degree from Beijing Jiaotong University, Beijing, China, in 2018, where he is currently pursuing the Ph.D. degree with the School of Automation and Intelligence. His research interests include modeling, optimal control, and optimization, with a specific emphasis on connected and automated vehicles.



Nikolce Murgovski is a Professor with the Department of Electrical Engineering, Division of Systems and Control, Chalmers University of Technology. He received the M.S. degree in Software Engineering from University West, Trollhättan, Sweden, in 2007, and the M.S. degree in Applied Physics and the Ph.D. degree in Systems and Control from the Chalmers University of Technology, Gothenburg, Sweden, in 2007 and 2012, respectively. His research interests are in optimization, optimal control, modelling, online learning and estimation. His typical research projects are within electromobility, autonomous driving and automotive active safety.



Wei Shangguan (Member, IEEE) received the B.S., M.S., and Ph.D. degrees from Harbin Engineering University, in 2002, 2005, and 2008, respectively. From 2013 to 2014, he was an Academic Visitor with University College London, London, U.K. He is currently a Professor with the School of Automation and Intelligence, Beijing Jiaotong University, Beijing, China. His research interests include autonomous intelligence, system modeling, simulation and testing, intelligent transportation systems, and train control systems.